

1 **Influence of Northeast Monsoon Cold Surges on Air Quality in Southeast Asia**

2

3 M. J. Ashfold^{a,*}, M. T. Latif^{b,c}, A. A. Samah^d, M. I. Mead^e, N. R. P. Harris^e

4 ^a School of Environmental and Geographical Sciences, University of Nottingham Malaysia Campus, 43500
5 Semenyih, Selangor, Malaysia

6 ^b School of Environmental and Natural Resource Sciences, Faculty of Science and Technology, Universiti
7 Kebangsaan Malaysia, 43600 Bangi, Selangor, Malaysia

8 ^c Institute for Environment and Development (Lestari), Universiti Kebangsaan Malaysia, 43600 Bangi,
9 Selangor, Malaysia

10 ^d Institute of Ocean and Earth Sciences, University of Malaya, 50603 Kuala Lumpur, Malaysia

11 ^e Centre for Atmospheric Informatics and Emissions Technology, Cranfield University, Cranfield, MK43 0AL,
12 United Kingdom

13 * Corresponding author: Matthew J. Ashfold (matthew.ashfold@nottingham.edu.my; +6 03 8725 3434)

14

15 **Abstract**

16 Ozone (O₃) is an important ground-level pollutant. O₃ levels and emissions of O₃ precursors have
17 increased significantly over recent decades in East Asia and export of this O₃ eastward across the
18 Pacific Ocean is well documented. Here we show that East Asian O₃ is also transported southward to
19 tropical Southeast (SE) Asia during the Northeast Monsoon (NEM) season (defined as November to
20 February), and that this transport pathway is especially strong during ‘cold surges’. Our analysis
21 employs reanalysis data and measurements from surface sites in Peninsular Malaysia, both covering
22 2003-2012, along with trajectory calculations. Using a cold surge index (northerly winds at 925 hPa
23 averaged over 105-110°E, 5°N) to define sub-seasonal strengthening of the NEM winds, we find the
24 largest changes in a region covering much of the Indochinese Peninsular and surrounding seas. Here,
25 the levels of O₃ and another key pollutant, carbon monoxide, calculated by the Monitoring

26 Atmospheric Composition and Climate (MACC) Reanalysis are on average elevated by, respectively,
27 >40% (~15 ppb) and >60% (~80 ppb) during cold surges. Further, in the broader region of SE Asia
28 local afternoon exceedances of the World Health Organization's air quality guideline for O₃ (100 μg
29 m⁻³, or ~50 ppb, averaged over 8 hours) largely occur during these cold surges. Day-to-day variations
30 in available O₃ observations at surface sites on the east coast of Peninsular Malaysia and in
31 corresponding parts of the MACC Reanalysis are similar, and are clearly linked to cold surges.
32 However, observed O₃ levels are typically ~10-20 ppb lower than the MACC Reanalysis. We show
33 that these observations are also subject to influence from local urban pollution. In agreement with past
34 work, we find year-to-year variations in cold surge activity related to the El Nino-Southern Oscillation
35 (ENSO), but this does not appear to be the dominant influence of ENSO on atmospheric composition
36 in this region. Overall, our study indicates that the influence of East Asian pollution on air quality in
37 SE Asia during the NEM could be at least as large as the corresponding, well-studied spring-time
38 influence on North America. Both an enhanced regional observational capability and chemical
39 modelling studies will be required to fully untangle the importance of this long-range influence
40 relative to local processes.

41

42 **Keywords:** Air quality; Ozone; Pollution; Northeast Monsoon; Southeast Asia

43

44 **Highlights**

- 45 ▪ Cold surges in November-February transport East Asian pollution to Southeast Asia
- 46 ▪ Regional exceedances of the WHO's O₃ guideline often occur during cold surges
- 47 ▪ Surface measurement sites in region also influenced by local sources of pollution
- 48 ▪ More observations in region and chemical modelling needed for further understanding

49

50 **1. Introduction**

51 Ground-level ozone (O₃) has important impacts on human health (Lelieveld et al., 2015), and these
52 impacts are likely to be large throughout the 21st century (Silva et al., 2016). In the tropical boundary

53 layer there are year-to-year variations in O₃ linked to the El Nino-Southern Oscillation (ENSO),
54 which modifies chemical and transport processes, and drives changes in emissions of O₃ precursors
55 (e.g. Inness et al., 2015; Hou et al., 2016). However, Ziemke et al. (2015) reported that variability in
56 tropical tropospheric O₃ is primarily driven by shorter timescale (non-ENSO) phenomena. One such
57 form of shorter-timescale variation is East Asian ‘cold surges’, characterised by periodic
58 strengthening of the prevailing north-easterly winds during the northern hemisphere (NH) winter
59 monsoon (or Northeast Monsoon, NEM), that have been studied for decades in a meteorological
60 context (e.g. Chang et al., 1979; Zhang et al., 1997). However, while past work (e.g. Liu et al., 2003;
61 Wang et al., 2016) has examined the influence of cold surges on atmospheric composition away from
62 the tropics, their importance for the tropics has received little attention.

63 This tropical impact could be large as during NH winter high levels of mid-latitude pollution found in
64 East Asia (e.g. Stein et al., 2014) are matched with unusually strong northerly winds towards the
65 equator. There is clearly great potential for significant transport of pollution to the deep tropics within
66 this particular range of longitudes, and this is particularly true during cold surge events. For example,
67 using trajectory calculations and observations for one NH winter Ashfold et al. (2015) showed that
68 cold surges could rapidly (over a few days) transport polluted air masses from East Asia to tropical
69 Southeast (SE) Asia. Oram et al. (unpublished results) present further measurements and model
70 results which demonstrate the likely importance of this mechanism for transporting large quantities of
71 short-lived chlorinated compounds, with the capacity to deplete stratospheric O₃, from East Asian
72 emission sources to the tropics.

73 Yet the spatial and temporal extent to which these cold surges affect air quality, including O₃ levels,
74 in SE Asia is not clear. It is well known that pollution originating in East Asia and transported
75 eastward leads to elevated O₃ levels above the North Pacific Ocean and in North America (e.g. Wild
76 and Akimoto, 2001; Liu et al., 2003; Zhang et al., 2008; Cooper et al., 2010; Lin et al., 2012; Lin et
77 al., 2014; Verstraeten et al., 2015), and so an equivalent impact in SE Asia linked to cold surges might
78 be expected. Such an impact is hinted at by Ashfold et al. (2015) who showed that cold surges could
79 increase O₃, as well as carbon monoxide (CO), another harmful gas that is often used as a marker for

80 anthropogenic pollution, to approximately double the levels typically found in the ‘clean’ background
81 atmosphere over the relatively short (~weeks-months) period covered by their analysis.

82 In this study we investigate more thoroughly the relationship between cold surges and SE Asian air
83 quality, with a particular focus on O₃, using longer-term datasets. We describe various aspects of our
84 methodology in Section 2. In Section 3.1 we provide a climatological background, and in Section 3.2
85 we characterize our cold surge index. Then in Section 3.3 we 1) use this index to explore air quality
86 composites for cold surge and non-cold surge conditions, 2) use dispersion model calculations to
87 further investigate the link between cold surges and high levels of pollution, and 3) consider the
88 importance of cold surges in driving exceedances of air quality thresholds in our study region on a
89 day-to-day basis. In Section 3.4 we compare reanalysis data with observations from surface sites. Our
90 final analysis, in Section 3.5, focuses on whether the known influence of ENSO on cold surge activity
91 is an important driver of year-to-year variations in pollution in SE Asia. Section 4 contains a
92 discussion of our key findings.

93

94 **2. Data and Methodology**

95 *2.1 Reanalysis data*

96 Much of our analysis relies on the Monitoring Atmospheric Composition and Climate (MACC)
97 Reanalysis of atmospheric composition (Inness et al., 2013), which has been used successfully in
98 studies of the tropical atmosphere (e.g. Inness et al., 2015; Ashfold et al., 2015). We extracted O₃, CO
99 and meridional wind (*v*) data for each November, December, January and February (NDJF) in the 10
100 year period covered by the dataset (2003-2012). We analyse time-steps at 06:00 and 18:00 Universal
101 Time (UT), or approximately 14:00 and 02:00 local time (LT). We consider a region covering tropical
102 SE Asia (90-125°E, 10°S-20°N), and extracted data with a horizontal resolution of 1.125° longitude
103 by 1.125° latitude, which is the native resolution of the chemical transport model within the reanalysis
104 system. We mostly present data on the 925 hPa pressure level, which is likely to be representative of
105 boundary layer conditions but less influenced by local surface processes than the alternative 1000 hPa

106 pressure level. Where necessary, we show that the choice of pressure level and time-step is not critical
107 to our conclusions. As well as gridded values, for purposes of comparison with observations, we use
108 bilinear interpolation to obtain MACC Reanalysis data for measurement site locations. Inness et al.
109 (2013) assessed the quality of the MACC Reanalysis through comparisons with independent
110 observations, and found modest negative biases of up to ~20% for O₃ through much of the tropical
111 troposphere, but slight positive biases (i.e. the reanalysis values were higher than the compared ozone
112 sonde values) below ~800 hPa. It is worth noting, however, the relative paucity of observations
113 available for validation in the region of the tropics covered by our study.

114 We also consider meridional wind data, for the same spatial region, from the ERA-Interim reanalysis
115 (Dee et al., 2011). We extracted a longer record, covering NDJF 1979-2015, at a horizontal resolution
116 of 0.75°, to enable a more thorough analysis of the wind regime in our study area. Bocquet et al.
117 (2015) note that the configuration of the MACC Reanalysis system is similar to that of ERA-Interim,
118 and indeed for our region of interest the winds in the two datasets are alike. For example, in Section
119 2.2 we describe an index for defining cold surges using meridional winds at 925 hPa, averaged over
120 105-110°E, at 5°N. Despite being interpolated from grids with different resolutions, the values of this
121 index over the period of the MACC reanalysis (2003-2012) in the two datasets are similar: coefficient
122 of determination, $r^2 = 0.98$ ($p < 0.001$), MACC mean = -5.4 m s^{-1} ; ERA-Interim mean = -4.8 m s^{-1} .

123 *2.2 Cold Surge definition*

124 There is no universal definition of a cold surge, with different authors typically using a definition that
125 best suits the geographical scope of their investigation. For example, Zhang et al. (1997) and Huang et
126 al. (2011) studied movement of the Siberian High – a typical feature of cold surge initiation – using
127 definitions based on aspects of sea level pressure and temperature over East Asia. In contrast, Chang
128 et al. (2005) studied the downstream impacts of cold surges on tropical convection and defined a cold
129 surge index using meridional wind at 925 hPa averaged over 110-117.5°E at 15°N. The same authors
130 defined a cold surge event when this index was stronger than -8 m s^{-1} . The definition of Chang et al.
131 (2005) was also adopted by Ooi et al. (2011), Hai et al. (2017) and, with slight modification, by
132 Juneng and Tanggang (2010) in their studies focused on the tropical atmosphere. In our analysis we

133 also employ the definition of Chang et al. (2005), which we will call V_{15} . As we are interested in
134 changes in composition in the deep tropics, and will make comparisons with air quality measurements
135 collected near 5°N in Peninsular Malaysia (see Section 2.4) we also define a second, similar index -
136 meridional wind at 925 hPa averaged over 105-110°E at 5°N - which we will call V_5 . In either case,
137 again in accordance with Chang et al. (2005), we define a cold surge event when $v < -8 \text{ m s}^{-1}$ (i.e.
138 when the magnitude of the northerly wind component is larger than 8 m s^{-1}).

139 *2.3 Dispersion model calculations*

140 To examine transport pathways associated with cold surges and variations in air quality we calculated
141 backward trajectories using the Numerical Atmospheric-dispersion Modelling Environment (NAME;
142 Jones et al., 2007), a Lagrangian particle dispersion model. Owing to the availability of driving
143 meteorological data we focus on calculations covering the final three complete NDJF seasons in the
144 MACC Reanalysis (i.e. November 2009-February 2010 to November 2011-February 2012). For each
145 3 hour period in these seasons, batches of 60,000 inert backward trajectories were started from a
146 source region covering the horizontal coordinates of the V_5 region (i.e. 105-110°E at 5°N) defined in
147 Section 2.2, and within an altitude range of 0-100 m. The trajectories were calculated over 12 days,
148 and every 15 minutes the location of all trajectories within the lowest 100 m of the model atmosphere
149 was recorded on a grid with a horizontal resolution of 0.5625° longitude by 0.375° latitude. The
150 model output on this grid was converted to an emission sensitivity – a quantitative measure of how
151 sensitive a receptor is to emissions in a grid cell – with units of s m^{-1} (i.e. $\text{g m}^{-3} / \text{g m}^{-2} \text{ s}^{-1}$). In addition
152 to the three seasons noted above, for illustration, we also present similar calculations for two specific
153 days: 13 and 23 January 2009.

154 The trajectories were calculated using three-dimensional meteorological fields produced by the UK
155 Meteorological Office's Numerical Weather Prediction tool, the Unified Model (UM). These fields
156 are available at 3 hour intervals and have varying spatial resolution. For calculations up to the end of
157 February 2010 they have a horizontal resolution of 0.5625° longitude by 0.375° latitude and 52
158 vertical levels below ~20 km. For calculations beginning in November 2010 they have a horizontal

159 grid resolution of $\sim 0.35^\circ$ longitude by $\sim 0.23^\circ$ latitude and 59 vertical levels below ~ 30 km. The sub-
160 grid scale process of turbulence is parameterised in NAME (Morrison and Webster, 2005).

161 *2.4 Surface air quality measurements*

162 For comparison with the MACC Reanalysis we also analyse O_3 and CO data from stations in a
163 network managed by Alam Sekitar Sdn Bhd (ASMA), a company which measures air quality on
164 behalf of the Malaysian Department of Environment (DOE). Covering more than 50 locations in
165 Malaysia around the southern edge of the South China Sea (SCS), the DOE network represents, to our
166 knowledge, the most widespread, long-term record of air quality in tropical SE Asia. Quality control
167 procedures for this network are described by Latif et al. (2014; their section 3.3) and ASMA (2007).
168 Observations from the DOE network have been analysed previously in several studies (e.g. Latif et
169 al., 2016 and references therein). Of importance here, Latif et al. (2014) have shown that even at the
170 designated ‘background’ station in this network, at Jerantut, there is evidence that local pollution (e.g.
171 from traffic) impacts the available observations. Accordingly, we will consider how useful the DOE
172 data are for studying the impact on air quality of large-scale meteorological processes such as cold
173 surges.

174 Our analysis of the DOE data focuses on three stations close to the east coast of Peninsular Malaysia,
175 at Kota Bharu (102.247°E , 6.141°N), Kuala Terengganu (103.118°E , 5.308°N) and Kemaman
176 (103.428°E , 4.271°N) (refer to Figure 6 to visualise locations). We believe these stations, lying in the
177 path of cold surges during the NEM, offer the best possibility of observing a cold surge influence on
178 air pollution within the DOE network. For each day considered in the MACC Reanalysis (i.e. in the
179 months of NDJF in the years 2003-2012), we compute ‘afternoon’ mean measured values by
180 averaging the 8 hourly mean values reported at 11:00-18:00 LT. An 8 hour averaging period is
181 commonly used in air quality regulations for O_3 , and we use this fixed ‘afternoon’ window 1) to
182 enable direct comparison with the 14:00 LT time-step in the MACC Reanalysis and 2) because it
183 typically captures peak O_3 values in the DOE network (see Latif et al., 2012; 2014). To avoid bias
184 where the peak in O_3 is not captured fully owing to missing data, we exclude days in which fewer
185 than 5 of the 8 hourly values are available.

186 2.5 Multivariate ENSO Index

187 We use the Multivariate ENSO Index (MEI, <https://www.esrl.noaa.gov/psd/enso/mei/>; Wolter and
188 Timlin, 1998) data for 1979-2015, which corresponds to the period covered in our analysis of ERA-
189 Interim data. When comparing the overlapping bimonthly MEI values with monthly fields we assume
190 the MEI value is valid for the second month (i.e. the MEI value for December-January is compared
191 with the January field of another dataset), as suggested here:
192 <https://www.esrl.noaa.gov/psd/enso/mei/table.html>. We also calculate seasonal means for NDJF by
193 averaging the bimonthly MEI values for October-November to January-February. Within the period
194 covered by the MACC Reanalysis (2003-2012) we categorise the three highest (MEI > 0.65) NDJF
195 seasonal mean values as El Nino winters (2004/05, 2006/07, 2009/10) and the three lowest (MEI < -
196 0.88) as La Nina winters (2007/08, 2010/11, 2011/12). This categorisation is consistent with that of
197 Inness et al. (2015).

198

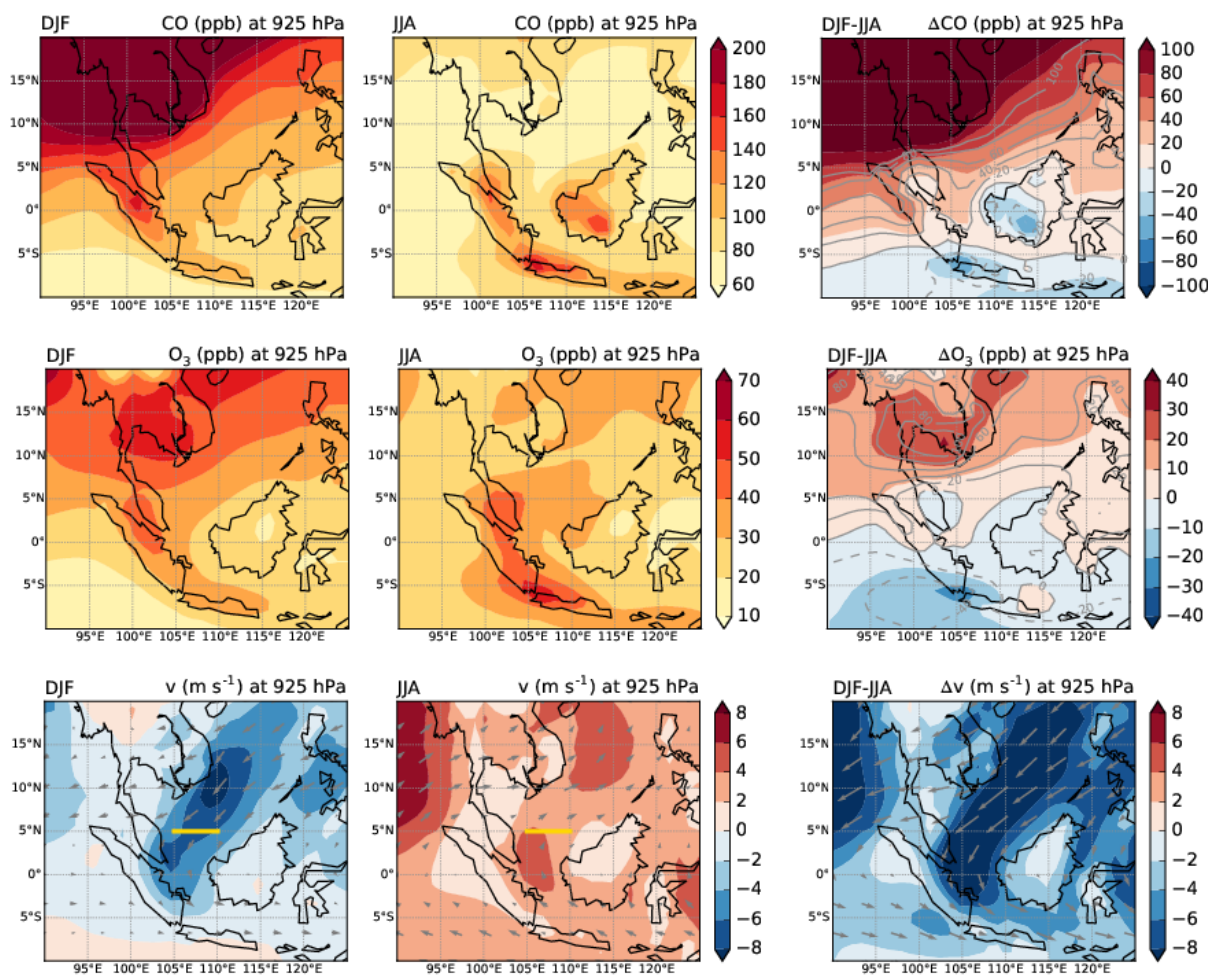
199 3. Results

200 3.1 Seasonal variations in atmospheric composition in SE Asia

201 To set the context for our analysis, we first examine seasonal differences in SE Asia for selected
202 variables in the MACC Reanalysis. Figure 1 shows a climatology of CO, O₃ and v for NH winter
203 (here using the common definition of the season, DJF) in SE Asia. For comparison, NH summer (JJA)
204 climatologies and the differences between the two seasons for the same variables are also shown. In
205 NH winter the strong (northerly component faster than 6 m s⁻¹) north-easterly monsoon winds over the
206 SCS are an obvious climatological feature. Also in NH winter levels of CO over much of Indochina
207 and the SCS are significantly higher (>100 ppb, or >100%) than in NH summer. The polluted air in
208 this region is likely linked to a combination of biomass burning during the dry season in Indochina
209 (e.g. Reid et al., 2013), longer chemical lifetimes in the winter hemisphere, and the phenomenon we
210 explore in more detail in subsequent sections – the transport by northerly winds of polluted air masses
211 from East Asia towards the tropics. Nearer the equator the situation is more mixed, with seasonal

212 differences (i.e. DJF-JJA) in equatorial parts of SE Asia typically smaller than ± 50 ppb for CO and
 213 ± 10 ppb for O₃. These smaller seasonal differences arise because there are regularly large near-
 214 equatorial sources of pollution during JJA, linked to landscape fires often occurring in parts of
 215 Indonesia (e.g. Reid et al., 2012; see the elevated climatological CO levels over Sumatra and southern
 216 Borneo in Figure 1). In Section 3.2 we focus on the northerly winds during NH winter, and explore
 217 the characteristics of cold surges in the context of this study. We then go on, in Section 3.3, to
 218 investigate the importance of pollution episodes in SE Asia linked to these cold surges.

219



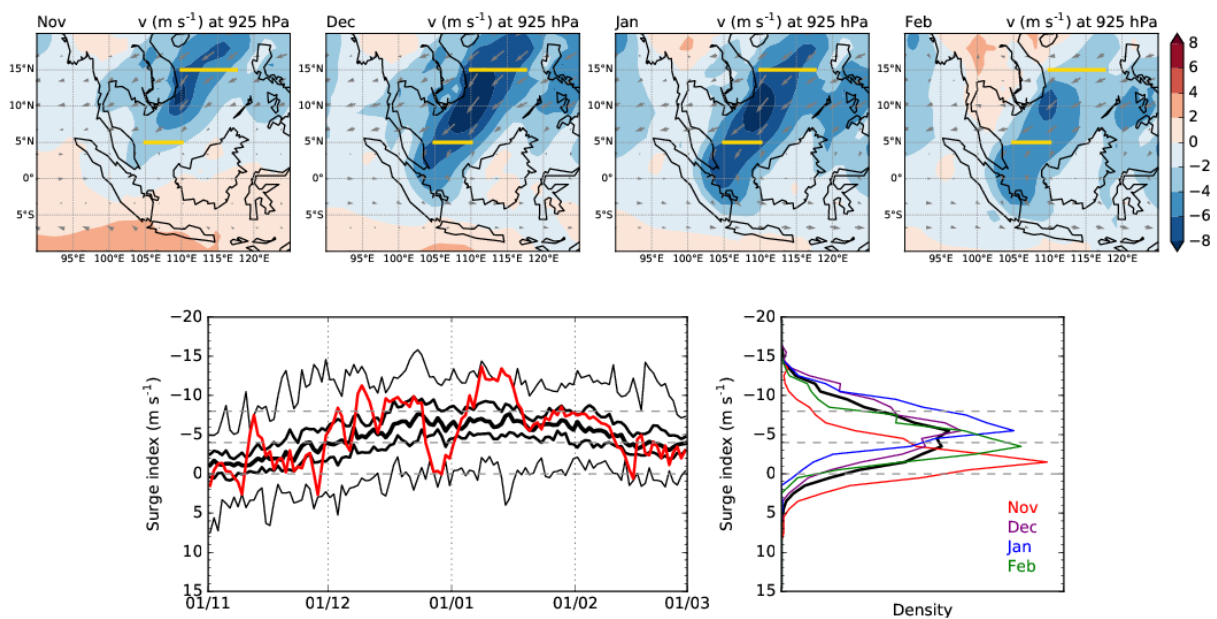
220

221 **Figure 1:** MACC Reanalysis CO (top), O₃ (middle) and meridional wind (bottom), all at 925 hPa, for DJF (left),
 222 JJA (centre) and DJF-JJA (right). The MACC data are averaged over 10 years (2003-2012). In the difference plots
 223 for CO and O₃ the shading shows absolute differences, and the labelled grey contours show percentage differences.
 224 The line over which the V₅ cold surge index, outlined in Section 2.2 and used in subsequent analyses, is calculated
 225 is marked in gold in the v panels.

226 3.2 NE monsoon winds and cold surges

227 In this section we examine the nature of changes in the northerly winds in the SCS during NH winter,
 228 with an emphasis on ‘cold surges’ as defined in Section 2.2. Considering month-by-month changes,
 229 Figure 2 shows that northerly winds in the SCS are generally strongest in December and January. The
 230 location of the strongest wind moves south along with the monsoon trough (approximately indicated
 231 by the transition from northerly to southerly winds; Reid et al., 2012) through the winter, so that the
 232 V_{15} cold surge index is strongest in December and weakens considerably by February, whereas V_5 is
 233 relatively weak in November and strengthens to a maximum in January. Clearly different measures of
 234 northerly winds will lead to somewhat different results, but overall we find that our key conclusions
 235 are not reliant on the choice of V_{15} or V_5 . We will focus on V_5 for our subsequent analysis, but given
 236 the strength of V_{15} during November (also see Zhang et al., 1997) we analyse NDJF as the relevant
 237 ‘seasonal’ period for cold surges rather than the typical DJF NH winter season.

238 Beyond the climatological situation, we will consider variability occurring over both day-to-day and
 239 year-to-year timescales. With respect to day-to-day variations, the red line in Figure 2 also shows,
 240 using the ENSO-neutral NH winter of 2008/09 as an illustrative example, that the strength of
 241 monsoon winds (as measured by V_5) during NDJF vary markedly around the average condition, with
 242 a clear illustration of a strong ($V_5 = -10$ – -12 m s^{-1}) cold surge in early-to-mid January 2009.



244 **Figure 2:** For November-February, the top row shows monthly mean maps of meridional wind (shading) and
245 wind vectors from the MACC Reanalysis. The lines over which two cold surges indices, V_5 and V_{15} , are calculated
246 are marked in gold. In the bottom row, the left panel shows daily mean values of V_5 from November 1 to February
247 28, with black lines denoting minimum, 25th, 50th and 75th percentile, and maximum values of the 37 years
248 (1979-2015) of ERA Interim data considered. The red line shows NDJF 2008/09 as an example. The right panel
249 shows corresponding monthly (November=red, December=purple, January=blue, February=green) and seasonal
250 (black) mean PDFs of V_5 . In both lower panels the V_5 stratifications used in subsequent analyses are marked with
251 dashed grey lines.

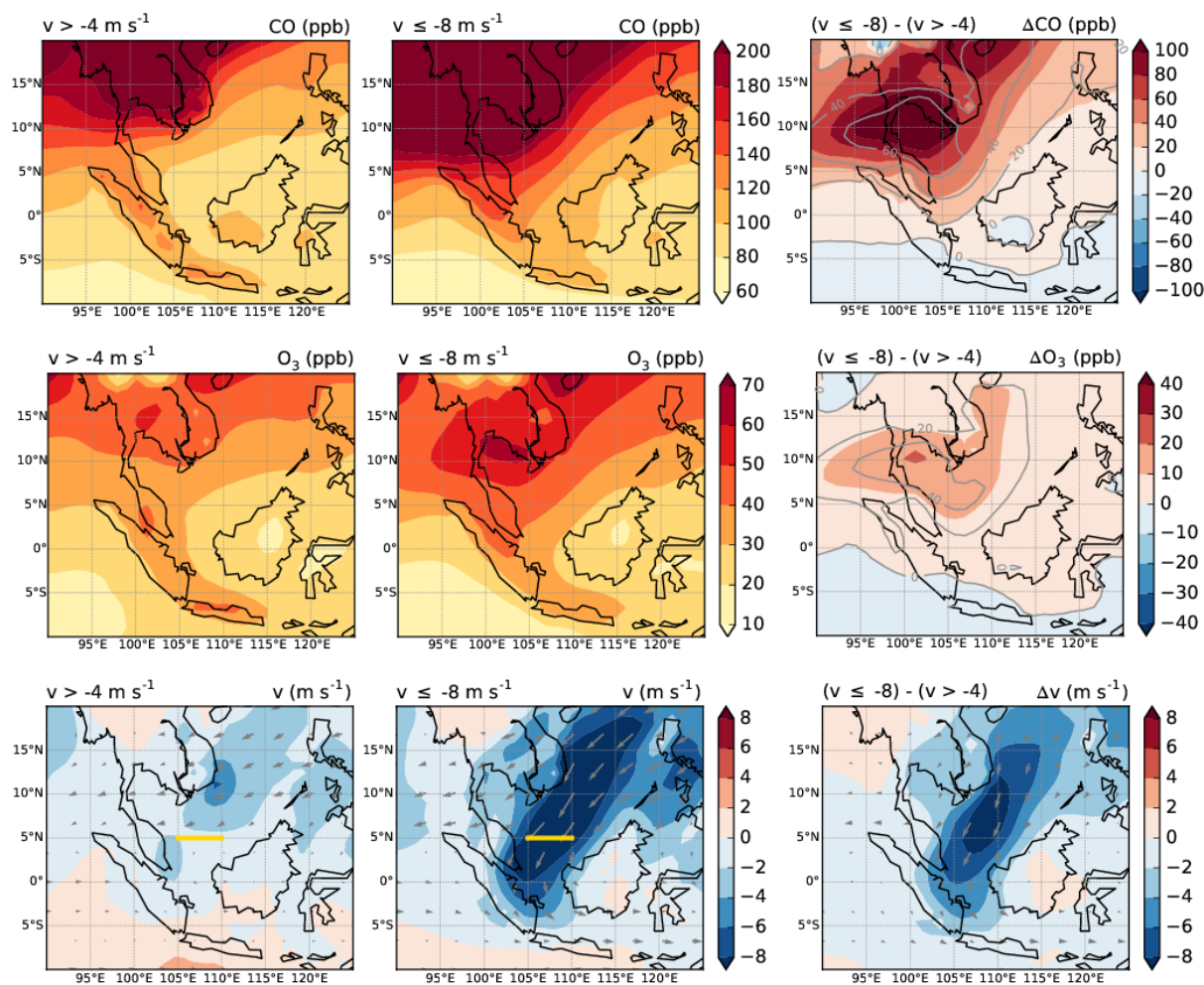
252

253 For further analysis we consider three stratifications of northerly wind. Similarly to Chang et al.
254 (2005) we define ‘cold surges’ as $V_5 < -8 \text{ m s}^{-1}$. We also define ‘weak’ winds as $V_5 > -4 \text{ m s}^{-1}$. Winds
255 between these two limits (i.e. $-8 < V_5 < -4 \text{ m s}^{-1}$) are closer to average. On a day-to-day basis through
256 the 37 years of the ERA-Interim Reanalysis we find that for V_5 , weak winds occur 42.2% of the time,
257 cold surge winds 17.9% of the time, and in between conditions 39.9% of the time. In the MACC
258 Reanalysis the corresponding values are 38.6%, 24.9% and 36.5%.

259 *3.3 Cold surges and atmospheric composition*

260 Using these three stratifications of northerly winds we now investigate variations in CO and O₃ in the
261 MACC Reanalysis dataset. Figure 3 presents composites of CO, O₃ and v for all days in the ‘cold
262 surge’ and ‘weak wind’ categories defined above, as measured by the V_5 index, along with the
263 difference between these two composites. There are, by definition, significant differences in v , which
264 are accompanied by large differences in atmospheric composition. In a region covering much of the
265 Indochinese Peninsular and surrounding seas CO and O₃ mixing ratios are elevated by, respectively,
266 >60% (~80 ppb) and >40% (~15 ppb), during cold surge conditions. Repeating this analysis using the
267 V_{15} index leads to similar patterns and conclusions, though the regions of maximum enhancements are
268 further from the equator (not shown). This analysis supports the general case for a significant
269 influence on variations in atmospheric composition in SE Asia by pollution within air masses
270 transported from outside the tropics.

271



272

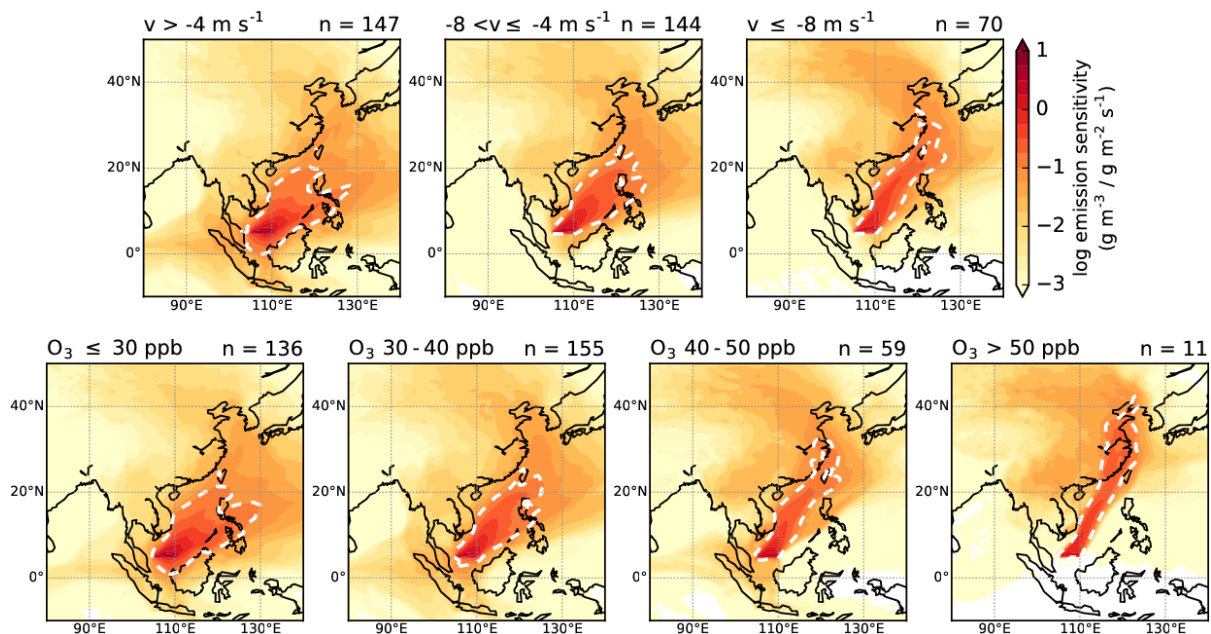
273 **Figure 3:** Composites for weak northerly winds (V_5 index $> -4 \text{ m s}^{-1}$, left column) and cold surge periods (V_5
 274 index $< -8 \text{ m s}^{-1}$, centre) and the difference between the two (right column) for CO (top), O_3 (middle) and v
 275 (bottom). The line over which V_5 is calculated is marked in gold in the v panels. In the difference plots for CO
 276 and O_3 the shading shows absolute differences, and the labelled grey contours show percentage differences.
 277 Constructed from twice daily (06UT and 18UT) MACC Reanalysis data for NDJF in the 10 years of the MACC
 278 Reanalysis (i.e. 1203 days). As noted in the main text, 39% of the time steps (929 of 2406) were classed as ‘weak
 279 wind’, 25% (600) were classed as ‘cold surge’ and 36% (877) were in between (i.e. $-8 < v < -4 \text{ m s}^{-1}$).

280

281 To explore further the link between transport from outside the tropics and variations in pollution in SE
 282 Asia we now examine trajectory calculations. Figure 4 shows composites, presented as emission
 283 sensitivities, for backward trajectories started in the V_5 region (see Section 2.3). The composites for
 284 the three V_5 stratifications demonstrate clear differences in air mass origin, with weaker V_5 winds
 285 linked to air travelling from the subtropical Pacific, and stronger winds (i.e. what we have defined as
 286 cold surge conditions) linked to transport of air from the East Asian landmass. In the latter case, the

287 transport pathway is consistent with the characteristic cold surge circulation pattern discussed by
 288 Ashfold et al. (2015), with strong northerly winds in the SCS leading to rapid meridional transport.
 289 This analysis suggests the V_5 index is a useful indicator of air mass origin. Next, consider the
 290 composites for four stratifications of MACC Reanalysis O_3 in the V_5 region (i.e. at 925 hPa, averaged
 291 over 105-110°E at 5°N). In the least polluted stratification (<30 ppb O_3), similar to the weak wind
 292 composite, back trajectories largely originate in the subtropical Pacific. In contrast, for the most
 293 polluted stratifications (40-50 ppb and >50 ppb O_3), similar to the cold surge composite, the dominant
 294 air mass source is the East Asian landmass. Together, this analysis links strong winds in the V_5 region
 295 with a cold surge circulation pattern, and with enhanced O_3 pollution in tropical SE Asia.

296



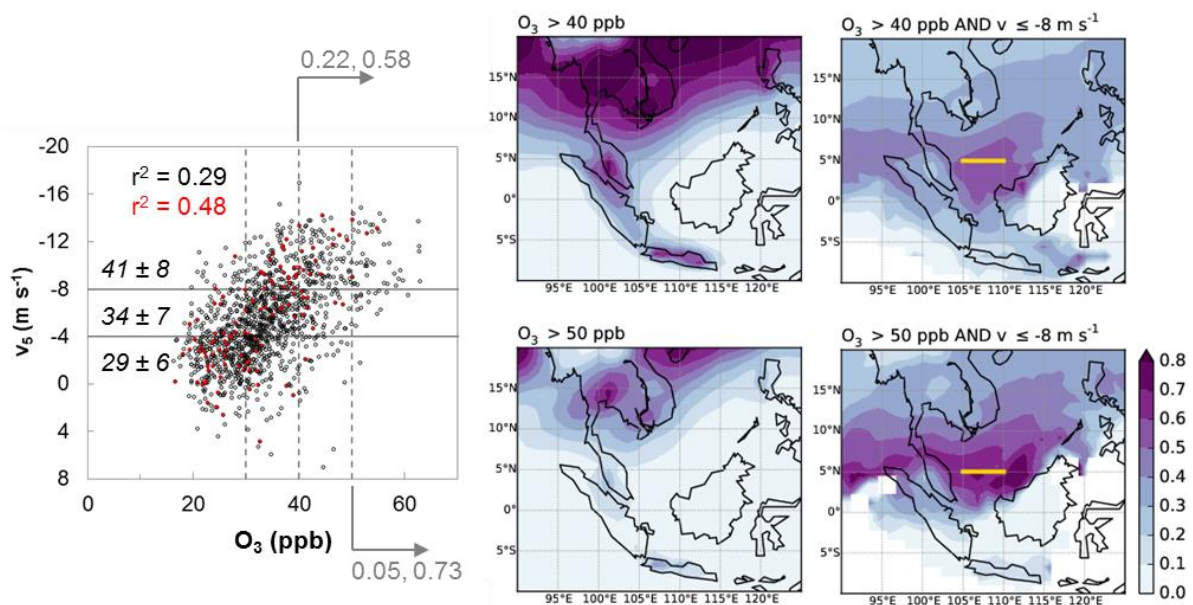
297

298 **Figure 4:** Composites of NAME emission sensitivity calculations for trajectories started in the V_5 region. The top
 299 row shows composites for the three V_5 stratifications discussed in Section 3.2 and used in Figure 3. The bottom
 300 row shows composites for four stratifications of MACC Reanalysis V_5 O_3 (from <30 ppb, left, to >50 ppb, right;
 301 these thresholds are used in Figure 5). The stratification label is given at the top-left of each panel. The number
 302 of days (n) contributing to each composite is marked at the top-right of each panel. To aid comparison the 10^{-1} (g
 303 $m^{-3} / g m^{-2} s^{-1}$) emission sensitivity contour is marked with a white dashed line. Constructed from the 361 days in
 304 the three complete NDJF seasons (2009/10-2011/12) for which both MACC Reanalysis and NAME data are
 305 available. The MACC data are for the 06:00 UT (14:00 LT) time-step, and the NAME trajectories considered
 306 were started between 03:00-09:00 UT (11:00-17:00 LT).

307

308 We next examine day-to-day variations in northerly winds and O₃ levels, with reference to air quality
 309 guidelines. Figure 5 shows the correlation ($r^2 = 0.29$ or $r = -0.54$, $p < 0.001$) between the V₅ index and
 310 corresponding O₃ levels (i.e. at 925 hPa, averaged over 105-110°E at 5°N; as used in Figure 4) at
 311 06:00 UT (14:00 LT) for each NDJF day in the ten years covered by the MACC Reanalysis (1203
 312 days in total). Considering the same three stratifications of v, mean (and standard deviation) O₃ values
 313 in this southerly part of the SCS are 29.0 (6.3) ppb for weak wind conditions, 34.2 (7.2) ppb for
 314 intermediate conditions, and 40.8 (8.3) ppb for cold surge conditions. In this V₅ region the World
 315 Health Organization's (WHO) Air Quality Guideline for O₃ (100 $\mu\text{g m}^{-3}$, i.e. a mixing ratio of ~50
 316 ppb) is exceeded just 5% of the time during NDJF, but 73% of these exceedances occur during cold
 317 surge conditions. Exceedances are therefore rare when winds from the north are weaker. The maps in
 318 Figure 5 indicate that exceedances of the 50 ppb O₃ threshold in much of this region, particularly in a
 319 band centred on 5°N, can be related to cold surge conditions in the V₅ region. Repeating this analysis
 320 using a lower O₃ threshold of 40 ppb (also in Figure 5), or a different cold surge definition (V₁₅ index,
 321 not shown), does not change this overall conclusion.

322



323

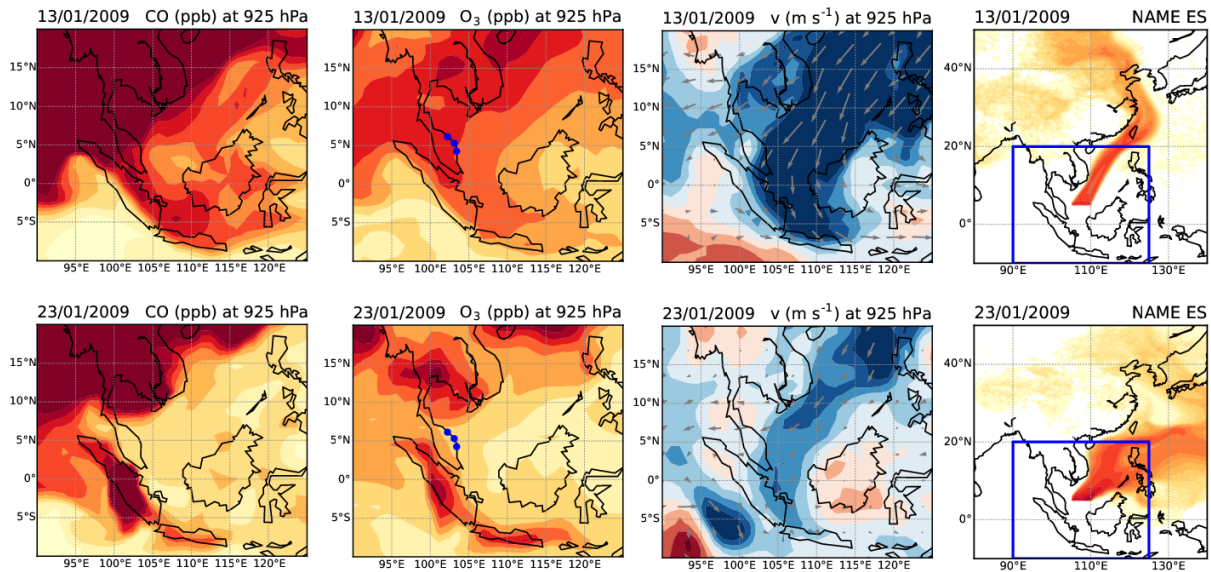
324 **Figure 5:** The left panel shows the correlation between MACC V₅ at 06:00 UT (14:00 LT) for each day in NDJF
 325 2003-2012 and O₃ values averaged over the same V₅ region. Illustrative values for NDJF 2008/09 are shown in
 326 red. Thresholds of 30, 40 and 50 ppb O₃ (as used in Figure 4) are marked with dashed lines. Mean and standard
 327 deviation O₃ values (in ppb) for the three northerly wind stratifications are noted in italics. Coefficient of
 328 determination (r^2) values for all NDJF months (black) and for 2008/09 (red) are noted to the top-left; $p < 0.001$ in

329 both cases. Right, maps showing the fraction (i.e. a number between 0 and 1) of days where the 06:00 UT (14:00
330 LT) O₃ values are higher than the 40 ppb and 50 ppb thresholds, and the sub-fraction of these days occurring
331 during cold surges ($V_5 < -8 \text{ m s}^{-1}$). The corresponding fractions related to the scatter plot (i.e. for O₃ averaged over
332 the V₅ region) are marked next to the arrows in grey text.

333

334 To illustrate the importance of cold surges in driving day-to-day variations in regional air quality,
335 Figure 6 shows regional patterns of MACC Reanalysis v, CO and O₃ along with NAME emission
336 sensitivities on two selected days, just 10 days apart. Along with the results in Figures 3, 4 and 5, this
337 figure demonstrates the large spatial scale of potential air quality impacts. In the case of 13 January
338 2009 strong northerly winds and associated polluted air from the East Asian landmass move far south
339 of the equator, reaching the coast of Java (~7°S). The situation on 23 January, when cleaner air
340 originating in the Pacific is found through most of the region, illustrates the marked variations in air
341 quality occurring over periods of days to weeks. In this context, it is also interesting to consider
342 specific locations, and so we compare MACC Reanalysis levels of O₃ on these two days averaged
343 over the V₅ region, and at Kota Bharu, the most northerly of the three surface sites considered in
344 Section 3.4. Consistent with the regional picture, O₃ levels are very different on the two days (44.3
345 ppb on 13 January and 20.8 ppb on 23 January in the V₅ region; 55.4 ppb and 28.9 at Kota Bharu), but
346 we emphasize that such O₃ levels, and the illustrative days selected, are not particularly unusual
347 within the 10 years of the MACC Reanalysis (respectively the 88th and 4th percentiles in the V₅ region,
348 and the 95th and 12th percentiles at Kota Bharu).

349



350

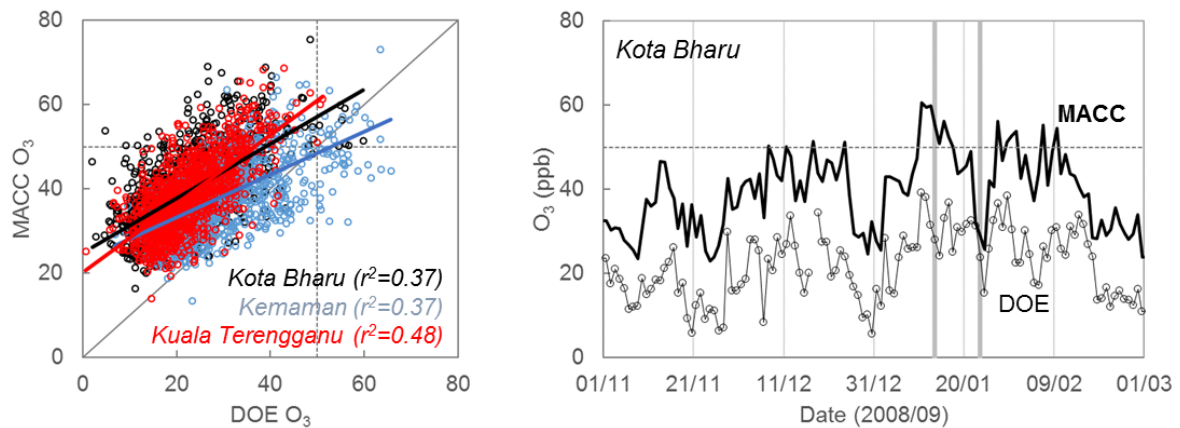
351 **Figure 6:** From left to right, examples of MACC Reanalysis data for CO, O₃ and v, and V₅ NAME emission
 352 sensitivities (ES), for 13 (top row) and 23 (bottom row) January 2009. The MACC data are at 925 hPa and the
 353 06:00 UT (14:00 LT) time-step. The NAME data are derived from trajectories started between 03:00–09:00 UT
 354 (11:00–17:00 LT). The locations of the three surface measurement sites considered in Figure 7 are marked with
 355 blue circles in the O₃ panels. The blue box in the NAME panels shows the area considered in the MACC panels.
 356 The colour scales are the same as those shown in Figure 3 (MACC data) and Figure 4 (NAME data).

357

358 3.4 Comparison of MACC Reanalysis and surface observations

359 To further examine the day-to-day air quality impacts in this region, we now compare the MACC
 360 Reanalysis data with observations from DOE surface sites. This analysis includes all NDJF months in
 361 the years 2003–2012. In Figure 7 the calculated daytime means of the DOE observations are compared
 362 with corresponding values from the MACC Reanalysis (14:00 LT, 925 hPa, interpolated to horizontal
 363 coordinates). The observations and the reanalysis exhibit similar day-to-day variability ($r^2 = 0.37–0.48$
 364 at the three sites, all $p < 0.001$), suggesting similar processes, linked to cold surges, are captured in
 365 both datasets. However, the measured O₃ levels are typically lower than predicted by MACC at all
 366 three sites (e.g. overall at Kota Bharu, mean DOE O₃ = 22.3 ppb and mean MACC O₃ = 39.5 ppb).
 367 One consequence of this difference is that while exceedances of the WHO’s Air Quality Guideline
 368 value of 50 ppb are often found (e.g. 50 ppb O₃ is the 87th percentile at Kota Bharu) within the MACC
 369 data, such breaches are much rarer (99th percentile) in the observations.

370



371

372 **Figure 7:** Left, considering all NDJF months in the years 2003-2012, the correlation between MACC and DOE
373 O₃ at the three DOE measurement sites: Kota Bharu (black), Kuala Terengganu (red) and Kemaman (blue). Lines
374 of best-fit are marked and r² values are noted; for all three sites p < 0.001. The locations of these three surface
375 sites are shown in Figure 5. Right, an illustrative time-series comparison for one NDJF season (November 2008-
376 February 2009) at Kota Bharu. DOE values are 8-hour averages of hourly mean values reported at 11:00-18:00
377 LT, while MACC values are for 06:00 UT (14:00 LT). The days presented in Figure 5 are marked with solid grey
378 lines. The WHO Air Quality Guideline for 8-hour average O₃ (50 ppb) is shown in both panels with a dashed line.

379

380 Why is there such a difference in magnitude between O₃ levels at the DOE sites, and the
381 corresponding MACC values? For consistency with earlier analyses we have used MACC data at 925
382 hPa, rather than 1000 hPa which may be more suitable for comparison with surface-based
383 observations. However, during local afternoon (14:00 LT), when the boundary layer is expected to be
384 relatively deep (see Samah et al., 2016), there is only a small difference between MACC O₃ values at
385 these two pressure levels (e.g. considering all NDJF in the MACC Reanalysis, for Kota Bharu: r² =
386 0.94, p < 0.001; 1000 hPa mean = 37.5 ppb, 925 hPa mean = 39.5 ppb). Another small difference is
387 created by comparing instantaneous MACC values with time-averaged observed values. To illustrate,
388 again at Kota Bharu, the average observed O₃ level reported at 14:00 LT (24.3 ppb) is 2 ppb higher
389 than the ‘afternoon mean’ value calculated over reports from 11:00-18:00 LT (22.3 ppb).

390 The remaining difference may be linked to the chemical regime in which the observations are made.

391 The DOE sites examined here measure air quality within, or on the edge of, urban centres of several
392 hundred thousand inhabitants, are several km from the coast, and data often exhibit characteristics of

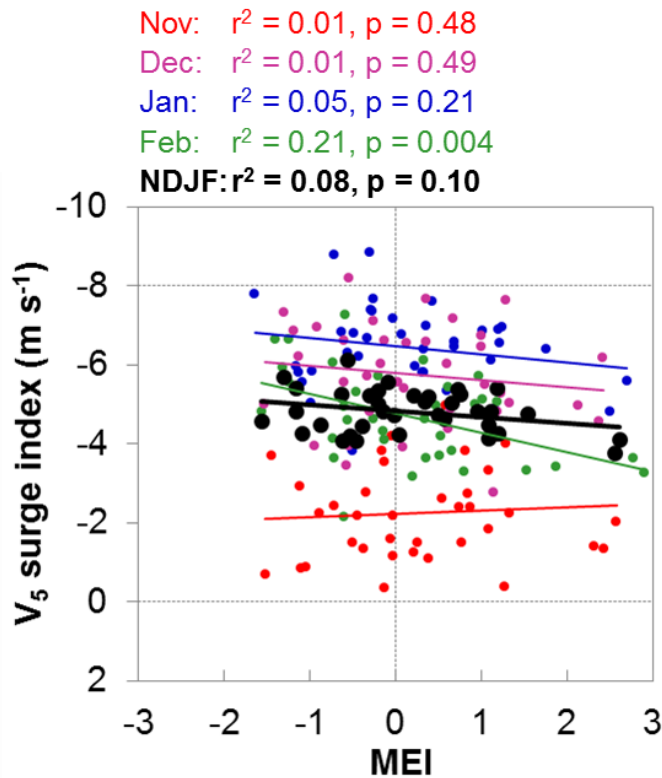
393 the polluted urban atmosphere. Measured daytime CO levels are significantly higher (e.g. mean ~500
394 ppb at Kota Bharu) than are found in the background atmosphere, or at the site locations within the
395 MACC Reanalysis, and some of the lowest measured O₃ values are associated with high levels (10s
396 ppb) of nitrogen oxides. In addition, while there is a strong positive relationship between O₃ and CO
397 in the MACC Reanalysis (for example, $r^2 = 0.66$, $p < 0.001$, at Kota Bharu), typical of regions of
398 pollution outflow (e.g. Chin et al., 1994; Voulgarakis et al., 2011), this relationship is much weaker in
399 the DOE measurements ($r^2 = 0.01$, $p < 0.001$, again at Kota Bharu). This strong evidence for some
400 local influence on the measured DOE O₃ values means it is difficult to be certain of the large-scale
401 representativeness of the DOE data; we return to this point in our discussion (Section 4).

402

403 *3.5 Year-to-year variation in the influence of cold surges*

404 We have shown that both ‘average’ and individual cold surges have an appreciable impact on levels
405 of O₃ as well as CO in a broad area of the SCS. We now consider whether there is year-to-year
406 variability in this impact. We begin by considering V₅ in relation to ENSO (as measured by the MEI).
407 Figure 8 shows a relatively weak relationship ($r^2 = 0.08$, $p = 0.10$) between the seasonal mean value of
408 V₅ and the corresponding seasonal mean value of the MEI. During La Nina (negative MEI values) NH
409 winters northerly winds are, on average, stronger than in El Nino winters. The ENSO influence on
410 northerly winds increases through the season from November ($r^2 = 0.01$; $r = -0.07$) to February ($r^2 =$
411 0.21 ; $r = 0.46$). The overall seasonal relationship is much stronger when V₁₅ is considered (seasonal r^2
412 $= 0.39$, $p < 0.001$) as are the individual monthly relationships (e.g. November $r^2 = 0.05$; February $r^2 =$
413 0.40), which, as for V₅, increase in strength through the season. This strong relation between ENSO
414 and V₁₅ is consistent with the analyses of Zhang et al. (1997) which focussed on regions somewhat
415 away from the equator. So it appears northerly winds further from the equator are more influenced by
416 the ENSO state, and it follows that northerly winds closer to the equator are less variable year-to-year.

417



418

419 **Figure 8:** Relationship between the Multivariate ENSO Index (MEI) and the V_5 index. NDJF seasonal (black)
 420 and monthly (November = red, December = purple, January = blue, February = green) mean values are presented.
 421 For each line of best fit a coefficient of determination (r^2) and associated p value are given. Constructed using
 422 ERA-interim data for November to February 1979-2015 (37 years, so 148 months in total) and MEI data.

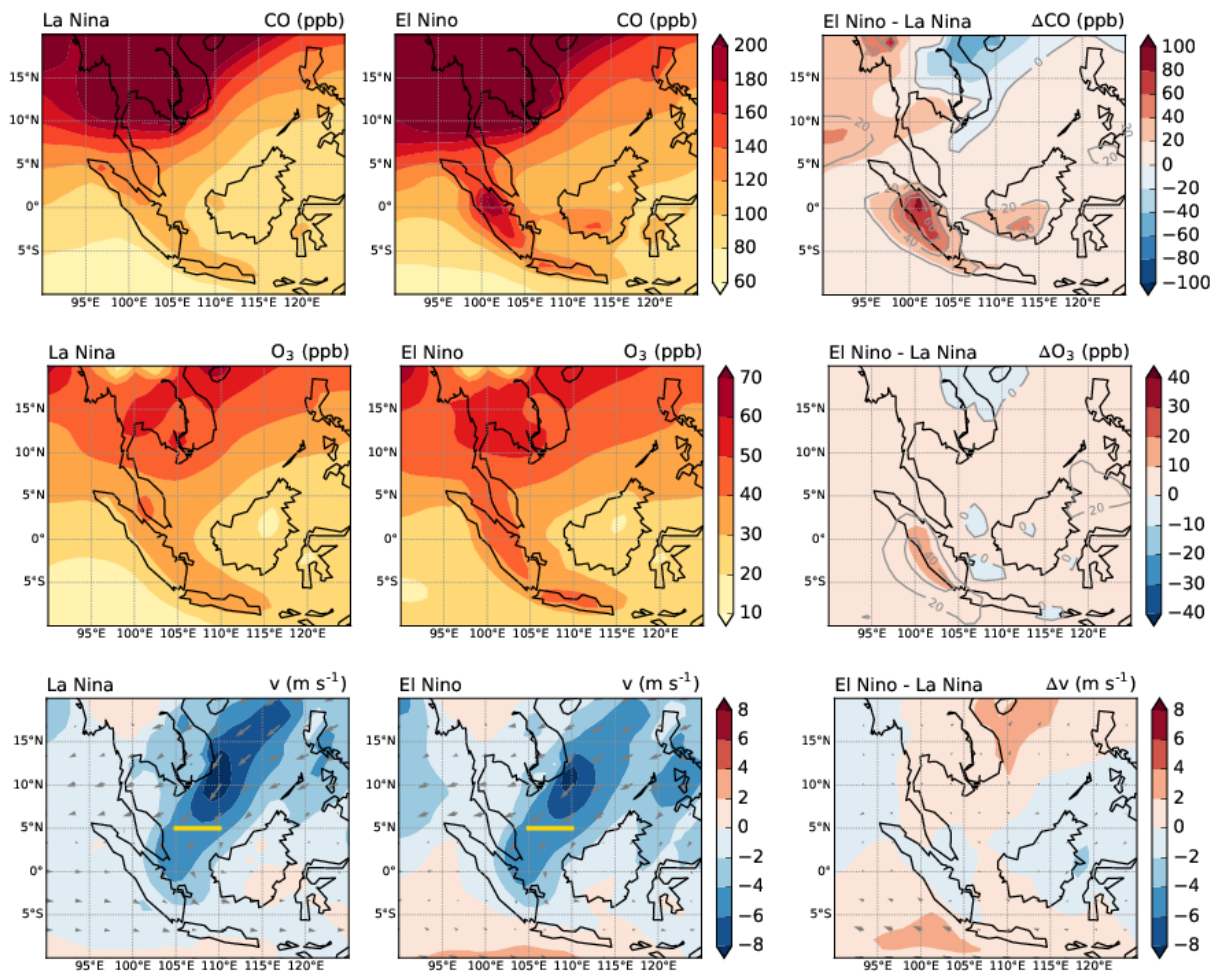
423

424 Given that during NH winter 1) ENSO has some influence on monthly and seasonal mean northerly
 425 winds in the SCS, and 2) the strength of northerly winds influences air quality in our study area, we
 426 might also expect corresponding year-to-year variability in levels of O_3 and CO. However, with the
 427 MACC Reanalysis covering a period of 10 years we have been able to define just three El Nino
 428 (2004/05, 2006/07, 2009/10) and three La Nina (2007/08, 2010/11, 2011/12) NDJF seasons in our
 429 analysis. This relatively short record, along with the fact that cold surges are not the only factor
 430 relevant to atmospheric composition that varies with respect to ENSO, mean that the analysis in the
 431 following paragraph ought to be considered an initial step towards answering this question.

432 In agreement with Figure 8, Figure 9 shows v in most of the SCS, and particularly further from the
 433 equator, is stronger in La Nina winters than in El Nino winters. However, Figure 8 also suggests that
 434 CO and O_3 are higher in La Nina winters only near the region over which the V_{15} index is calculated.

435 In most other parts of SE Asia pollutant levels are higher during El Nino winters. For example, Figure
 436 9 shows elevated CO over Sumatra which is an indicator of landscape fires that, although more
 437 frequent from June-October (Reid et al., 2012), can occur during the NEM season (e.g. during
 438 February 2005 and November 2006). This analysis suggests that, while perceptible, year-to-year
 439 variations in cold surge activity are not the dominant influence of ENSO on atmospheric composition
 440 in most of this region during NDJF. Conversely, it is also worth noting that landscape fires occurring
 441 during El Nino NH winters can partly obscure the role of cold surges (e.g. in our analysis in Figure 3).
 442 If we repeat that analysis but exclude the winters of 2004/05 and 2006/07 (where, as noted above,
 443 there were significant fires in Sumatra) then the pollution anomaly – particularly for CO – associated
 444 with strong northerly winds is further enhanced just south of the equator (not shown).

445



446

447 **Figure 9:** Composites for La Nina (left) and El Nino (centre) and the difference between the two (right) for CO
448 (top), O₃ (middle) and v (bottom). The line over which V₅ is calculated is marked in gold in the v panels. In the
449 difference plots the shading shows absolute differences, and the labelled grey contours show percentage
450 differences. Composites for El Nino and La Nina were constructed from, respectively, the three highest and three
451 lowest seasonal MEI values (averaged over the October-November, November-December, December-January,
452 and January-February values) in the nine complete NDJF seasons in the MACC Reanalysis.

453

454 **4. Discussion and Conclusions**

455 Our analysis of MACC Reanalysis data, along with the supporting trajectory calculations, has shown
456 that NEM cold surges have a significant impact on aspects of air quality in SE Asia. The largest
457 impact is in a region covering much of the Indochinese Peninsular and surrounding seas, where CO
458 and O₃ are elevated by, respectively, >60% (~80 ppb) and >40% (~15 ppb), during ‘average’ cold
459 surge conditions (using the V₅ definition). In much of this area, and indeed also in the wider SE Asia
460 region, exceedances of the WHO’s Air Quality Guideline value for O₃ of 50 ppb mostly occur during
461 cold surge periods. It is of interest to compare these results with studies examining the influence of
462 pollution originating in East Asia on O₃ in North America. For example, Zhang et al. (2008)
463 diagnosed a ground-level O₃ enhancement due to Asian pollution, covering most of the western half
464 of continental USA during NH spring, of 5-7 ppb. For the same season and region, Lin et al. (2012)
465 found that Asian pollution contributed 8-15 ppb on days when surface O₃ exceeded 60 ppb. As such,
466 the seasonal influence of East Asian pollution on air quality in Southeast Asia could be at least as
467 large as the corresponding, well-studied influence on North America. Zhang et al. (2008), and later
468 both Cooper et al. (2010) and Lin et al. (2017), also demonstrated a growing influence of East Asian
469 pollution on O₃ in North America. It seems reasonable to speculate that a similar trend will have
470 affected our region of study. Zhang et al. (2016) showed large increases in O₃ over SE Asia between
471 1980-2010, but did not explore the details of pollution transport within the region in different seasons.
472 Within this work, it is difficult to demonstrate conclusive evidence for such trends because 1) our ten
473 year analysis period is shorter than ideal for this type of investigation, and 2) some potentially
474 complicating discontinuities exist within the MACC Reanalysis (see Inness et al., 2013; Bocquet et
475 al., 2015). Detailed studies with chemical transport models will help to isolate the importance of East

476 Asian pollution for this region, as well as to examine the relative impact of changes in East Asian
477 pollutant emissions and changes in regional circulation patterns (e.g. Cai et al., 2017).

478 We also showed that available O₃ observations at DOE surface sites on the east coast of Peninsular
479 Malaysia and equivalent MACC Reanalysis data exhibit similar day-to-day variability, linked to cold
480 surges, but that measured O₃ levels are typically lower. The measured levels of CO and nitrogen
481 oxides and their correlations with O₃ are indicative of a competing influence from local urban
482 pollution, and suggest that it is difficult to be certain of the large-scale representativeness of the DOE
483 data. Comprehensive surface observations from a truly ‘background’ site would therefore be
484 extremely desirable for studying the impact of long-range transport of pollution in cold surges on
485 atmospheric composition in SE Asia. Indeed, Sofen et al. (2016) suggest that for O₃, this region –
486 typical of tropical areas – is not characterised at all by existing measurement sites. One candidate is
487 the research station established recently by the University of Malaya at Bachok, a rural area on the
488 coast 25 km southeast of the Kota Bharu site considered here, which Oram et al. (unpublished results)
489 show is subject to appreciable pollution from East Asia during cold surges. The physical properties of
490 the lower atmosphere (e.g. the mixing height) at sites in this region are modified by cold surges (e.g.
491 Samah et al., 2016), and the importance of these modifications for atmospheric composition needs to
492 be understood. Further, any coastal site in this region is likely to be strongly affected by diurnal sea
493 breeze circulations (see Qian et al., 2013), and indeed Dominick et al. (2015) have shown that this
494 type of circulation could be important in controlling particulate matter concentrations at the Bachok
495 site. These points, along with rapid regional urbanization (Schneider et al., 2015) in largely coastal
496 cities, encourages further examination of coastal processes in the tropics related to air quality, which
497 are not likely to be fully captured in a relatively coarse resolution product such as the MACC
498 Reanalysis employed here.

499 In agreement with past studies (e.g. Zhang et al., 1997) we found year-to-year variations in cold surge
500 activity linked to ENSO. In our analysis the relationship between ENSO and meridional wind was
501 stronger further from the equator and later in the season. However, our analysis also shows that
502 variations in cold surge activity do not appear to be the dominant influence of ENSO on atmospheric

503 composition in most of the region. Instead, changes in emissions from fires, known to be influenced
504 by ENSO-related variations in regional climate, appear to be more important (e.g. Reid et al., 2012;
505 Inness et al., 2015; Voulgarakis et al., 2015).

506 Though we have mostly focussed on variations in O₃, cold surges also clearly lead to significant
507 enhancements in CO (e.g. Figure 3), a gas with industrial sources that is known to be well correlated
508 with a range of other anthropogenic pollutants (e.g. Shao et al., 2011). For some gases, such as
509 chlorinated very short-lived substances (e.g. dichloromethane, CH₂Cl₂) that have the potential to
510 contribute to stratospheric O₃ depletion, the pollutant source distribution is likely to be more
511 dominated by the mid-latitudes than is the case for CO, and so the signature of NEM cold surges on
512 this aspect of atmospheric composition in SE Asia will be proportionately larger. Measurements of a
513 wider range of anthropogenically influenced gases in this season and region will therefore be of great
514 interest.

515

516 **Acknowledgments**

517 This research was supported by NERC International Opportunities Fund project NE/J016012/1. We
518 acknowledge use of the NAME atmospheric dispersion model and associated NWP meteorological
519 data sets made available to us by the UK Met Office. We also acknowledge the significant storage
520 resources and analysis facilities made available to us on JASMIN by STFC CEDA along with the
521 corresponding support teams. We are grateful for use of data provided by the MACC-II project,
522 funded by the European Union under the 7th Framework Programme. We also thank the Malaysian
523 Department of Environment for providing the air quality observations. The constructive comments of
524 two anonymous reviewers and Mr Ooi See Hai (University of Malaya) are also gratefully
525 acknowledged.

526

527

528

529 **References**

- 530 Ashfold, M. J.; Pyle, J. A.; Robinson, A. D.; Meneguz, E.; Nadzir, M. S. M.; Phang, S. M.; Samah, A.
531 A.; Ong, S.; Ung, H. E.; Peng, L. K.; Yong, S. E. & Harris, N. R. P. Rapid transport of East Asian
532 pollution to the deep tropics. *Atmospheric Chemistry and Physics*, 2015, 15, 3565-3573.
- 533 ASMA, Standard Operating Procedure for Continuous Air Quality Monitoring. Selangor: Alam
534 Sekitar Sdn. Bhd. Shah Alam; 2007.
- 535 Bocquet, M.; Elbern, H.; Eskes, H.; Hirtl, M.; Žabkar, R.; Carmichael, G. R.; Flemming, J.; Inness,
536 A.; Pagowski, M.; Pérez Camaño, J. L.; Saide, P. E.; San Jose, R.; Sofiev, M.; Vira, J.; Baklanov, A.;
537 Carnevale, C.; Grell, G. & Seigneur, C. Data assimilation in atmospheric chemistry models: current
538 status and future prospects for coupled chemistry meteorology models. *Atmospheric Chemistry and*
539 *Physics*, 2015, 15, 5325-5358.
- 540 Cai, W.; Li, K.; Liao, H.; Wang, H. & Wu, L. Weather conditions conducive to Beijing severe haze
541 more frequent under climate change. *Nature Climate Change*, 2017, 7, 257-262.
- 542 Chang, C.-P.; Erickson, J. E. & Lau, K. M. Northeasterly Cold Surges and Near-Equatorial
543 Disturbances over the Winter MONEX Area during December 1974. Part I: Synoptic Aspects.
544 *Monthly Weather Review*, 1979, 107, 812-829.
- 545 Chang, C.-P.; Harr, P. A. & Chen, H.-J. Synoptic Disturbances over the Equatorial South China Sea
546 and Western Maritime Continent during Boreal Winter. *Monthly Weather Review*, 2005, 133, 489-
547 503.
- 548 Chin, M.; Jacob, D. J.; Munger, J. W.; Parrish, D. D. & Doddridge, B. G. Relationship of ozone and
549 carbon monoxide over North America. *Journal of Geophysical Research*, 1994, 99, 14565-14573.
- 550 Cooper, O. R.; Parrish, D. D.; Stohl, A.; Trainer, M.; Nedelec, P.; Thouret, V.; Cammas, J. P.;
551 Oltmans, S. J.; Johnson, B. J.; Tarasick, D.; Leblanc, T.; McDermid, I. S.; Jaffe, D.; Gao, R.; Stith, J.;
552 Ryerson, T.; Aikin, K.; Campos, T.; Weinheimer, A. & Avery, M. A. Increasing springtime ozone
553 mixing ratios in the free troposphere over western North America. *Nature*, 2010, 463, 344-348.
- 554 Dee, D. P.; Uppala, S. M.; Simmons, A. J.; Berrisford, P.; Poli, P.; Kobayashi, S.; Andrae, U.;
555 Balmaseda, M. A.; Balsamo, G.; Bauer, P.; Bechtold, P.; Beljaars, A. C. M.; van de Berg, L.; Bidlot,
556 J.; Bormann, N.; Delsol, C.; Dragani, R.; Fuentes, M.; Geer, A. J.; Haimberger, L.; Healy, S. B.;
557 Hersbach, H.; Hólm, E. V.; Isaksen, I.; Kållberg, P.; Köhler, M.; Matricardi, M.; McNally, A. P.;
558 Monge-Sanz, B. M.; Morcrette, J.-J.; Park, B.-K.; Peubey, C.; de Rosnay, P.; Tavalato, C.; Thépaut,
559 J.-N. & Vitart, F. The ERA-Interim reanalysis: configuration and performance of the data assimilation
560 system. *Quarterly Journal of the Royal Meteorological Society*, 2011, 137, 553-597.
- 561 Dominick, D.; Latif, M. T.; Juneng, L.; Khan, M. F.; Amil, N.; Mead, M. I.; Nadzir, M. S. M.; Moi, P.
562 S.; Samah, A. A.; Ashfold, M. J.; Sturges, W. T.; Harris, N. R. P.; Robinson, A. D. & Pyle, J. A.
563 Characterisation of particle mass and number concentration on the east coast of the Malaysian
564 Peninsula during the northeast monsoon. *Atmospheric Environment*, 2015, 117, 187-199.
- 565 Hai, O. S.; Samah, A. A.; Chenoli, S. N.; Subramaniam, K. & Ahmad Mazuki, M. Y. Extreme
566 Rainstorms that Caused Devastating Flooding across the East Coast of Peninsular Malaysia during
567 November and December 2014. *Weather and Forecasting*, 2017, 32, 849-872.

568 Hou, X.; Zhu, B.; Fei, D.; Zhu, X.; Kang, H. & Wang, D. Simulation of tropical tropospheric ozone
569 variation from 1982 to 2010: The meteorological impact of two types of ENSO event *Journal of*
570 *Geophysical Research: Atmospheres*, 2016, 121, 9220-9236.

571 Huang, W.-R.; Wang, S.-Y. & Chan, J. C. L. Discrepancies between global reanalyses and
572 observations in the interdecadal variations of Southeast Asian cold surge *International Journal Of*
573 *Climatology*, 2011, 31, 2272-2280.

574 Inness, A.; Baier, F.; Benedetti, A.; Bouarar, I.; Chabrillat, S.; Clark, H.; Clerbaux, C.; Coheur, P.;
575 Engelen, R. J.; Errera, Q.; Flemming, J.; George, M.; Granier, C.; Hadji-Lazaro, J.; Huijnen, V.;
576 Hurtmans, D.; Jones, L.; Kaiser, J. W.; Kapsomenakis, J.; Lefever, K.; Leitão, J.; Razinger, M.;
577 Richter, A.; Schultz, M. G.; Simmons, A. J.; Suttie, M.; Stein, O.; Thépaut, J.-N.; Thouret, V.;
578 Vrekoussis, M.; Zerefos, C. & the MACC team. The MACC reanalysis: an 8 yr data set of
579 atmospheric composition. *Atmospheric Chemistry and Physics*, 2013, 13, 4073-4109.

580 Inness, A.; Benedetti, A.; Flemming, J.; Huijnen, V.; Kaiser, J. W.; Parrington, M. & Remy, S. The
581 ENSO signal in atmospheric composition fields: emission-driven versus dynamically induced
582 changes. *Atmospheric Chemistry and Physics*, 2015, 15, 9083-9097.

583 Jones, A.; Thomson, D.; Hort, M. & Devenish, B. The U.K. Met Office's Next-Generation
584 Atmospheric Dispersion Model, NAME III. *Air Pollution Modeling and Its Application XVII*,
585 Borrego, C. & Norman, A.-L. (Eds.), Springer US, 2007, 580-589.

586 Juneng, L. & Tangang, F. T. Long-term trends of winter monsoon synoptic circulations over the
587 maritime continent: 1962—2007. *Atmospheric Science Letters*, 2010, 11, 199-203.

588 Latif, M. T.; Huey, L. S. & Juneng, L. Variations of surface ozone concentration across the Klang
589 Valley, Malaysia. *Atmospheric Environment*, 2012, 61, 434 - 445

590 Latif, M. T.; Dominick, D.; Ahamad, F.; Khan, M. F.; Juneng, L.; Hamzah, F. M. & Nadzir, M. S. M.
591 Long term assessment of air quality from a background station on the Malaysian Peninsula. *Science*
592 *of The Total Environment*, 2014, 482-483, 336-348.

593 Latif, M. T.; Dominick, D.; Ahamad, F.; Ahamad, N. S.; Khan, M. F.; Juneng, L.; Xiang, C. J.;
594 Nadzir, M. S. M.; Robinson, A. D.; Ismail, M.; Mead, M. I. & Harris, N. R. P. Seasonal and long term
595 variations of surface ozone concentrations in Malaysian Borneo. *Science of The Total Environment*,
596 2016, 573, 494-504.

597 Lelieveld, J.; Evans, J. S.; Fnais, M.; Giannadaki, D. & Pozzer, A. The contribution of outdoor air
598 pollution sources to premature mortality on a global scale. *Nature*, 2015, 525, 367-371.

599 Lin, M.; Fiore, A. M.; Horowitz, L. W.; Cooper, O. R.; Naik, V.; Holloway, J.; Johnson, B. J.;
600 Middlebrook, A. M.; Oltmans, S. J.; Pollack, I. B.; Ryerson, T. B.; Warner, J. X.; Wiedinmyer, C.;
601 Wilson, J. & Wyman, B. Transport of Asian ozone pollution into surface air over the western United
602 States in spring. *Journal of Geophysical Research*, 2012, 117.

603 Lin, M.; Horowitz, L. W.; Oltmans, S. J.; Fiore, A. M. & Fan, S. Tropospheric ozone trends at Mauna
604 Loa Observatory tied to decadal climate variability. *Nature Geoscience*, 2014, 7, 136-143.

605 Lin, M.; Horowitz, L. W.; Payton, R.; Fiore, A. M. & Tonnesen, G. US surface ozone trends and
606 extremes from 1980 to 2014: quantifying the roles of rising Asian emissions, domestic controls,
607 wildfires, and climate. *Atmospheric Chemistry and Physics*, 2017, 17, 2943-2970.

608 Liu, H.; Jacob, D. J.; Bey, I.; Yantosca, R. M.; Duncan, B. N. & Sachse, G. W. Transport pathways
609 for Asian pollution outflow over the Pacific: Interannual and seasonal variations. *Journal Of*
610 *Geophysical Research*, 2003, 108, 8786.

611 Morrison, N. L. & Webster, H. N. An Assessment of Turbulence Profiles in Rural and Urban
612 Environments Using Local Measurements and Numerical Weather Prediction Results. *Boundary-*
613 *Layer Meteorology*, 2005, 115, 223-239.

614 Oman, L. D.; Ziemke, J. R.; Douglass, A. R.; Waugh, D. W.; Lang, C.; Rodriguez, J. M. & Nielsen, J.
615 E. The response of tropical tropospheric ozone to ENSO. *Geophysical Research Letters*, 2011, 38,
616 L13706.

617 Ooi, S. H.; Samah, A. A. & Braesicke, P. A case study of the Borneo Vortex genesis and its
618 interactions with the global circulation. *Journal Of Geophysical Research*, 2011, 116, D21116.

619 Oram, D. E.; Ashfold, M. J.; Laube, J. C.; Gooch, L. J.; Humphrey, S.; Sturges, W. T.; Leedham-
620 Elvidge, E.; Forster, G. L.; Harris, N. R. P.; Mead, M. I.; Samah, A. A.; Phang, S. M.; Ou-Yang, C.-
621 F.; Lin, N.-H.; Wang, J.-L.; Baker, A. K.; Brenninkmeijer, C. A. M.; Sherry, D. A growing threat to
622 the ozone layer from short-lived anthropogenic chlorocarbons. *Atmospheric Chemistry and Physics*
623 *Discussions*, in review, 2017, 1-20, doi:10.5194/acp-2017-497.

624 Qian, J.-H.; Robertson, A. W. & Moron, V. Diurnal Cycle in Different Weather Regimes and Rainfall
625 Variability over Borneo Associated with ENSO. *Journal Of Climate*, 2013, 26, 1772-1790.

626 Reid, J. S.; Xian, P.; Hyer, E. J.; Flatau, M. K.; Ramirez, E. M.; Turk, F. J.; Sampson, C. R.; Zhang,
627 C.; Fukada, E. M. & Maloney, E. D. Multi-scale meteorological conceptual analysis of observed
628 active fire hotspot activity and smoke optical depth in the Maritime Continent. *Atmospheric*
629 *Chemistry and Physics*, 2012, 12, 2117-2147.

630 Reid, J. S.; Hyer, E. J.; Johnson, R. S.; Holben, B. N.; Yokelson, R. J.; Zhang, J.; Campbell, J. R.;
631 Christopher, S. A.; Di Girolamo, L.; Giglio, L.; Holz, R. E.; Kearney, C.; Miettinen, J.; Reid, E. A.;
632 Turk, F. J.; Wang, J.; Xian, P.; Zhao, G.; Balasubramanian, R.; Chew, B. N.; Janjai, S.; Lagrosas, N.;
633 Lestari, P.; Lin, N.-H.; Mahmud, M.; Nguyen, A. X.; Norris, B.; Oanh, N. T.; Oo, M.; Salinas, S. V.;
634 Welton, E. J. & Liew, S. C. Observing and understanding the Southeast Asian aerosol system by
635 remote sensing: An initial review and analysis for the Seven Southeast Asian Studies (7SEAS)
636 program. *Atmospheric Research*, 2013, 122, 403-468.

637 Samah, A. A.; Babu, C.; Varikoden, H.; Jayakrishnan, P. & Hai, O. S. Thermodynamic and dynamic
638 structure of atmosphere over the east coast of Peninsular Malaysia during the passage of a cold surge.
639 *Journal of Atmospheric and Solar-Terrestrial Physics*, 2016, 146, 58-68.

640 Schneider, A.; Mertes, C. M.; Tatem, A. J.; Tan, B.; Sulla-Menashe, D.; Graves, S. J.; Patel, N. N.;
641 Horton, J. A.; Gaughan, A. E.; Rollo, J. T.; Schelly, I. H.; Stevens, F. R. & Dastur, A. A new urban
642 landscape in East-Southeast Asia, 2000-2010. *Environmental Research Letters*, 2015, 10, 034002.

643 Shao, M.; Huang, D.; Gu, D.; Lu, S.; Chang, C. & Wang, J. Estimate of anthropogenic halocarbon
644 emission based on measured ratio relative to CO in the Pearl River Delta region, China. *Atmospheric*
645 *Chemistry and Physics*, 2011, 11, 5011-5025.

646 Sheel, V.; Sahu, L. K.; Kajino, M.; Deushi, M.; Stein, O. & Nedelec, P. Seasonal and interannual
647 variability of carbon monoxide based on MOZAIC observations, MACC reanalysis, and model
648 simulations over an urban site in India. *Journal of Geophysical Research: Atmospheres*, 2014,
649 2013JD021425.

650 Silva, R. A.; West, J. J.; Lamarque, J.-F.; Shindell, D. T.; Collins, W. J.; Dalsoren, S.; Faluvegi, G.;
651 Folberth, G.; Horowitz, L. W.; Nagashima, T.; Naik, V.; Rumbold, S. T.; Sudo, K.; Takemura, T.;
652 Bergmann, D.; Cameron-Smith, P.; Cionni, I.; Doherty, R. M.; Eyring, V.; Josse, B.; MacKenzie, I.
653 A.; Plummer, D.; Righi, M.; Stevenson, D. S.; Strode, S.; Szopa, S. & Zengast, G. The effect of future
654 ambient air pollution on human premature mortality to 2100 using output from the ACCMIP model
655 ensemble. *Atmospheric Chemistry and Physics*, 2016, 16, 9847-9862.

656 Sofen, E. D.; Bowdalo, D. & Evans, M. J. How to most effectively expand the global surface ozone
657 observing network. *Atmospheric Chemistry and Physics*, 2016, 16, 1445-1457.

658 Stein, O.; Schultz, M. G.; Bouarar, I.; Clark, H.; Huijnen, V.; Gaudel, A.; George, M. & Clerbaux, C.
659 On the wintertime low bias of Northern Hemisphere carbon monoxide found in global model
660 simulations. *Atmospheric Chemistry and Physics*, 2014, 14, 9295-9316.

661 Verstraeten, W. W.; Neu, J. L.; Williams, J. E.; Bowman, K. W.; Worden, J. R. & Boersma, K. F.
662 Rapid increases in tropospheric ozone production and export from China. *Nature Geoscience*, 2015, 8,
663 690-695.

664 Voulgarakis, A.; Telford, P. J.; Aghedo, A. M.; Braesicke, P.; Faluvegi, G.; Abraham, N. L.;
665 Bowman, K. W.; Pyle, J. A. & Shindell, D. T. Global multi-year O₃-CO correlation patterns from
666 models and TES satellite observations. *Atmospheric Chemistry and Physics*, 2011, 11, 5819-5838.

667 Voulgarakis, A.; Marlier, M. E.; Faluvegi, G.; Shindell, D. T.; Tsigaridis, K. & Mangeon, S.
668 Interannual variability of tropospheric trace gases and aerosols: The role of biomass burning
669 emissions. *Journal of Geophysical Research: Atmospheres*, 2015, 120, 7157-7173.

670 Wang, Z.; Liu, X. & Xie, X. Effects of Strong East Asian Cold Surges on Improving the Air Quality
671 over Mainland China. *Atmosphere*, 2016, 7, 38.

672 Wild, O. & Akimoto, H. Intercontinental transport of ozone and its precursors in a three-dimensional
673 global CTM. *Journal of Geophysical Research: Atmospheres*, 2001, 106, 27729-27744.

674 Wolter, K. & Timlin, M. S. Measuring the strength of ENSO events: How does 1997/98 rank?
675 *Weather*, 1998, 53, 315-324.

676 Zhang, Y.; Sperber, K. R. & Boyle, J. S. Climatology and Interannual Variation of the East Asian
677 Winter Monsoon: Results from the 1979-95 NCEP/NCAR Reanalysis. *Monthly Weather Review*,
678 1997, 125, 2605-2619.

679 Zhang, L.; Jacob, D. J.; Boersma, K. F.; Jaffe, D. A.; Olson, J. R.; Bowman, K. W.; Worden, J. R.;
680 Thompson, A. M.; Avery, M. A.; Cohen, R. C.; Dibb, J. E.; Flock, F. M.; Fuelberg, H. E.; Huey, L.
681 G.; McMillan, W. W.; Singh, H. B. & Weinheimer, A. J. Transpacific transport of ozone pollution
682 and the effect of recent Asian emission increases on air quality in North America: an integrated
683 analysis using satellite, aircraft, ozonesonde, and surface observations. *Atmospheric Chemistry and*
684 *Physics*, 2008, 8, 6117-6136.

685 Zhang, Y.; Cooper, O. R.; Gaudel, A.; Thompson, A. M.; Nedelec, P.; Ogino, S.-Y. & West, J. J.
686 Tropospheric ozone change from 1980 to 2010 dominated by equatorward redistribution of emissions.
687 *Nature Geoscience*, 2016, 9, 875-879.

688 Ziemke, J. R.; Douglass, A. R.; Oman, L. D.; Strahan, S. E. & Duncan, B. N. Tropospheric ozone
689 variability in the tropics from ENSO to MJO and shorter timescales. *Atmospheric Chemistry and*
690 *Physics*, 2015, 15, 8037-8049.

Influence of Northeast Monsoon cold surges on air quality in Southeast Asia

Ashfold, Matthew J.

2017-07-27

Attribution-NonCommercial-NoDerivatives 4.0 International

M.J. Ashfold, M.T. Latif, A.A. Samah, M.I. Mead, N.R.P. Harris, Influence of Northeast Monsoon cold surges on air quality in Southeast Asia, In Atmospheric Environment, Volume 166, 2017, Pages 498-509

<https://doi.org/10.1016/j.atmosenv.2017.07.047>

Downloaded from CERES Research Repository, Cranfield University